Journal Homepage: -www.journalijar.com

INTERNATIONAL JOURNAL OF ADVANCED RESEARCH (IJAR)

Article DOI:10.21474/IJAR01/24519
DOI URL: http://dx.doi.org/10.21474/IJAR01/24519

RESEARCH ARTICLE

PETROGRAPHIC AND GEOCHEMICAL CHARACTERIZATION OF GRANITOIDS FROM THE BAGAROUA-FIANGA LOCALITY (MAYO KEBBI MASSIF) IN SOUTHWESTERN CHAD: SOURCE AND GEODYNAMIC CONTEXT

Gustave Baïssemia Ronang[1], Klamadji Moussa Ngarena[1] and Mbaguedje Diondoh[2]

1. Department of Mining and Geological Engineering, Faculty of Life and Earth Sciences, Pala University, P.O. Box. 20, Pala, Chad.
2. Adam Barka University of Abeché, Department of Earth Sciences, Chad.

Manuscript Info

Manuscript History
Received: 04 September 2026
Final Accepted: 08 October 2026
Published: November 2026

Key words:-
Bagaroua-Fianga, Mayo Kebbi Massif, fractional crystallization, geodynamics, southwestern Chad

Abstract

The Bagaroua - Fianga massif in Mayo Kebbi consists of granodiorite, granite, metadiorite, and metagabbro. These are shoshonitic and calc-alkaline in type,with moderate potassium content. The metagabbros and metadiorites are rich in magnesium,while the granites and granodiorites are magnesian and ferrous. Fractional crystallization processes are indic ated by petrology, geochemistry, and field relationships. The enrichmen t in LREE relative to HREE (La_N/Yb_N varying between 1.42–3.19) and the flat profile (Dy_N/Yb_N varying between 0.80–1.31) of HREE in the rocks of the Bagaroua-Fianga massif lead us to propose that these rocks originate from fractional crystallization of mantle rocks. Consequently, granodiorites are found as enclaves within granites. The linear associati on between granites and the intermediate location of granodiorite and metagabbro enclaves leads us to suggest magmatic hybridization as the predominant process that drove the evolution of granitoids and metagabbros in the Mayo Kebbi massif. The partial melting of the subduction-altered mantle and lower continental crust was likely triggered by the delamination of the continental lithosphere during the post-collisional stage of the Pan-African orogeny, which led to the formation of the granitoid magmas present in the Mayo Kebbi Massif.

"© 2026 by the Author(s). Published by IJAR under CC BY 4.0. Unrestricted use allowed with credit to the author."

Introduction:-

The Mayo Kebbi orogenic chain is part of the Central African Pan-African Chain (CAPC), which underwent remobilization during the Pan-African orogeny between 700 and 500 Ma [1]. The CPAC is located between the Congo Craton and the Sahara Metacraton (Fig. 1) and is the result of the convergence of the West African and Congo-Sao Francisco Cratons, as highlighted by[2]. This chain is connected to the Borborema region in northeastern Brazil, which is also part of the Neoproterozoic Brasiliano Belt [3, 4, 5]. Numerous studies focusing on tectonics and associated magmatic activities have led to the assertion of a collision between continents in the CAPC[6, 7].

In Chad, the CAPC consists of Precambrian formations divided into five massifs: (1) the Tibesti massif in the north, formed of Pan-African granites [8], and a metamorphic Paleoproterozoic unit dominated by metasedimentary

Corresponding Author:- Gustave Baïssemia Ronang
Address:- Department of Mining and Geological Engineering, Faculty of Life and Earth Sciences, Pala University, P.O. Box. 20, Pala, Chad.

formations[9]; (2) the Ouaddaï massif in the east, composed of an Archean to Paleoproterozoic crust remobilized during the Pan-African orogeny and a juvenile Neoproterozoic crust[10, 11, 12]; (3) the Guéra massif in the center of the country, which encompasses a Neoproterozoic crust made up of Pan-African calc-alkaline granites[13, 14]; (4) The Baïbokoum massif in the far south has a Neoproterozoic crust composed of calc-alkaline granite and syenites containing metasedimentary and amphibolite enclaves[15, 16]. (5) The Mayo Kebbi massif in the southwest is characterized by a juvenile Neoproterozoic crust composed, from bottom to top, of: (a) a mafic to ultramafic plutonic grouping, (b) belts of green metasedimentary-metavolcanic rocks, (c) various calc-alkaline granites, accumulated in an intra-oceanic arc setting during successive phases of expansion and contraction[17, 18]. Although several studies have been conducted in the western section of the Mayo Kebbi massif (Leré), the meta-mafic rocks located in the east (Goueïgoudoum) remain largely unexplored in terms of geochemistry.

In this paper, we present petrographic and geochemical data (major elements, trace elements, and rare earth elements) relating to the metamafic and granitoid rocks of the eastern section of the Mayo Kebbi massif (Bagaroua-Fianga). The objective is to determine their provenance, establish their tectonic context, and compare them with other granitoids from Precambrian formations in Chad.

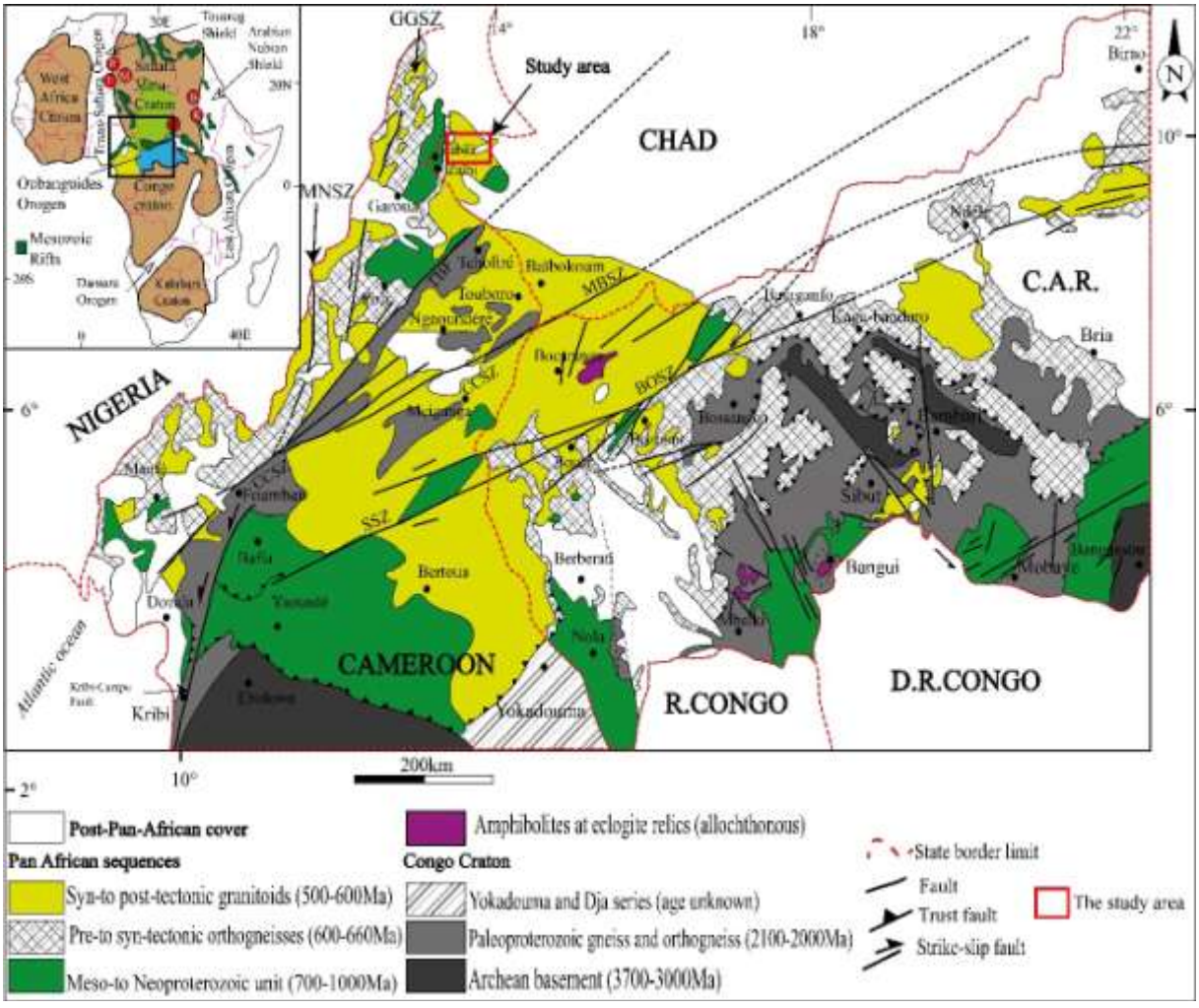


Figure 1: Geological map of Central Africa (based on [19, 20, 21, 22, 23, 24, 25, 26]highlights the main litho-tectonic units and zones of the Central African Orogenic Belt (SZ - Shear Zone; CCSZ - Central Cameroon Shear Zone; MNSZ - Mayo Nolti Shear Zone; SSZ - Sanaga Shear Zone; MBSZ - M'Béré Shear Zone; BOSZ - Bozoum-Ndélé Shear Zone; TBF - Tcholliré Banyo Fault; CAR - Central African Republic; R.Congo - Republic of Congo; DRC - Democratic Republic of Congo).

Geological context of the Bagaroua-Fianga massif:-

The Bagaroua-Fianga massif (Fig. 2) in Mayo-Kébbi is an elongated NE-SW feature located between the Central Cameroon and North Cameroon domains. It differs from these two domains in its juvenile Neoproterozoic crust [17, 18, 27, 28, 29, 30]). In the southeast, it is separated from the Central Cameroon domain by the Massenia-Ounianga gravimetric anomaly, which is an extension of the Tcholliré-Banyo shear zone [27,30, 31]. It is separated from the North Cameroon domain by the Zalbi volcano-sedimentary chain, which is considered to be a northeastern extension of the Poli group [31]. This domain corresponds to a magmatic arc zone that formed between 800 Ma and 550 Ma through successive collisions with the Central Cameroon and North Cameroon domains, respectively [17]. It comprises: (1) Greenstone belts comprising volcanosedimentary series (Gouegoudoum in the east and Zalbi in the west) and a complex of mafic to intermediate rocks (metadiorite, metagabbro-diorite, and metagabbro) dated to around 748 Ma and 700 Ma, respectively.

These rocks are deformed and metamorphosed in green schist facies. They result from juvenile accretion in an island arc or back-arc basin context. (2) The Mayo-Kebbi batholith consists of three generations of granitoids: (i) the syn-tectonic quartzite metadiorite of the Gauchiot Falls magmatic complex dated to 665 ± 1 Ma, whose emplacement is contemporary with the first collision involving the Mayo-Kébbi domain and the Central Cameroon domain. This collision marks the beginning of crustal thickening and the closure of the Zalbi back-arc basin; (ii) hornblende and biotite tonalites dated to 647 ± 5 Ma, formed by partial melting of green rocks and syn-tectonic quartzic metadiorites; and (iii) syn-tectonic tonalites dated to 618 Ma, formed during the second collision between the Mayo-Kebbi/Central Cameroon block and the North Cameroon domain; and (3) There are two types of post-tectonic intrusions: post-tectonic calc-alkaline potassium granites and alkaline granites. The former resulted from the partial melting of the lower crust [32]. Alkaline granites result from extreme fractional crystallization of mantle magma contaminated by Archean to Paleoproterozoic crust during its ascent [18]. These two types of granite formed in green rocks around 570 Ma (U/Pb zircon[18, 33].

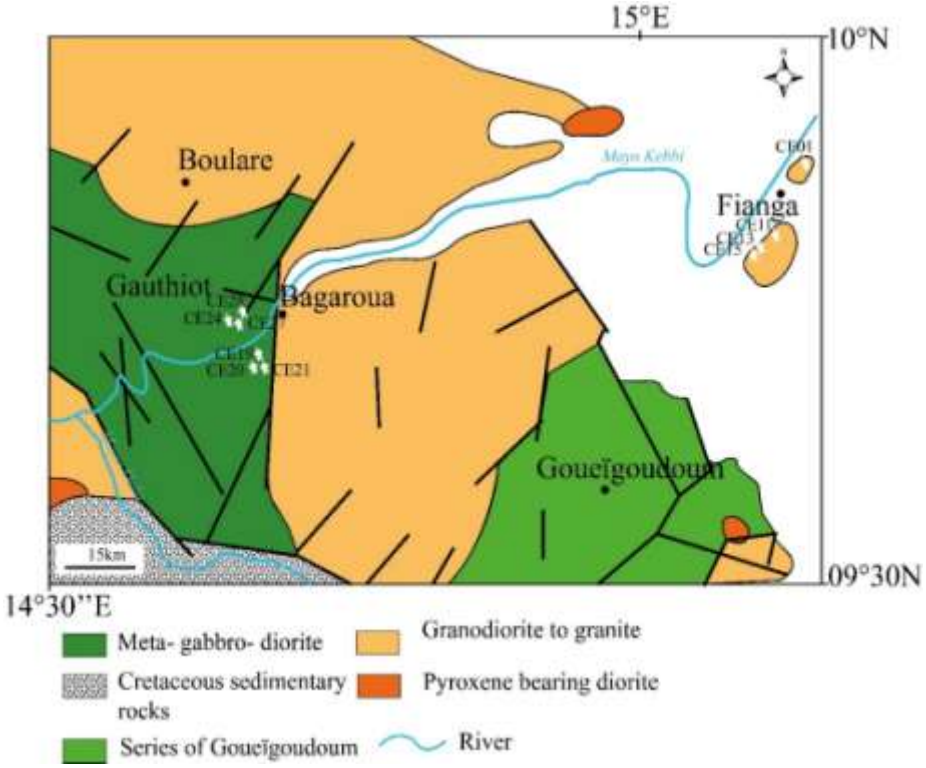


Figure 2: Geological map of the study area

Analytical method:-

The chemical composition of whole rock was determined for 10 rock samples collected from the Mayo Kebbi massif using ICP-AES methods. This technique was used to measure the major elements and some trace elements in the rock samples. All analyses were performed at the ALS Geochemistry-Loughrea Ireland laboratory, which is

equipped with an inductively coupled plasma emission spectrometer (ICP-AES). Chemical analyses of whole rocks were performed, and the results are presented in Table 1. Data on major and trace elements from the Bagaroua and Fianga massif are listed in Table 1. Whole rock analyses of major elements were performed by inductively coupled plasma atomic emission spectrometry (ICP-AES) and trace elements were analyzed by inductively coupled plasma mass spectrometry (ICP-MS) from pastes. 0.2 g of rock powder was fused with 1.5 g of $LiBO_2$ and then dissolved in 100 mm 35% HNO_3. REE contents were determined by ICP-MS from pastes after dissolving 0.25 g of rock powder with 4 acid digestions. Analytical precisions range from 0.1% to 0.02% for major elements; from 0.01 to 0.5 ppm for trace elements; and from 0.01 to 5 ppm for rare earth elements.

Results:-

Petrography:-

Granodiorite:-

Granodiorites outcrop as enclaves in granites (Fig. 3a). The rock texture is granular, rich in ferromagnesian minerals (biotite, amphibole) and poor in felsic minerals (quartz, alkali feldspar). Under the microscope, the microstructure of granodiorite is porphyroid, mainly rich in plagioclase, biotite, amphibole, and interstitial crystals of feldspar and quartz (Fig. 3b). Plagioclase (50%) is generally sub-rectangular with regular or corroded contours. Polysynthetic albite twinning is common, but sporadically, polysynthetic albite twinning and Carlsbad twinning, synneusis accolades, or concentric zoning are observed. Inclusions of biotite flakes, hornblende crystals, titanite, apatite, and opaque minerals are observed in the plagioclase. Damourite alteration is noted. Alkaline feldspars (10–15%) appear as sub-tabular Carlsbad twinned crystals (orthoclase). Inclusions are represented by biotite lamellae and crystals of titanite, apatite, hornblende, and opaque minerals. Alteration to sericite is noted on some potassium feldspar crystals. Quartz (10–15%) occurs as irregularly shaped crystals exhibiting weak undulating extinction. It is also observed in interstitial sections between feldspar crystals. Biotite, apatite, and opaque minerals constitute the inclusions in quartz. Biotite (8–10%) occurs as brown subtabular flakes with strong pleochroism in dark brown. It often forms crystal aggregates with hornblende and opaque minerals. The cleavage marks are clear but sometimes highlighted by exsolutions of opaque oxides. Locally, biotite flakes border the alkaline feldspars and plagioclase. The biotite flakes contain numerous inclusions of zircon, titanite, and opaque minerals. The amphibole (3–5%) is dark green to greenish yellow in color, reminiscent of green hornblende. It occurs as sub-rectangular or irregular crystals. Green hornblende crystals locally exhibit h1 twinning. They are associated with opaque minerals, titanite crystals, and biotite flakes.

Granite:-

Granite outcrops in blocks and slabs (Fig. 3c). Under the microscope, granite has a porphyroid grain texture with a mineralogical composition consisting of potassium feldspar, quartz, plagioclase, and biotite. Accessory mineral phases are represented by apatite, zircon, titanite, and opaque minerals (Fig. 3d). The sub-tabular crystals of potassium feldspars (30–40%) have irregular boundaries. However, Carlsbad twinned orthoclase crystals are also observed, which locally exhibit a transformation into microcline. Biotite, plagioclase, and opaque minerals are frequently observed inclusions. They are locally altered and replaced by sericite. Quartz (20–30%) occurs locally in elongated sections with sinuous contours and weak undulating extinction. Inclusions are represented by biotite, titanite, and opaque minerals. Plagioclase (15–18%) occurs as sub-tabular crystals. They frequently exhibit polysynthetic twinning of albite, but sometimes polysynthetic twinning of albite and Carlsbad twinning are also observed. Some plagioclase crystals show exsolutions of fine quartz vermicules (myrmekites) at their edges in contact with adjacent potassium feldspars. Biotite (5–8%) is light brown to greenish brown and strongly pleochroic in dark brown and greenish brown. Biotite is locally altered to form pale green chlorite at its edges or along its cleavage traces.

Metagabbro:-

Metagabbro occurs in dark-colored blocks (Fig. 3e), with blurred boundaries between them and neighboring lithologies. Under the microscope, metagabbros (Fig. 3f) display a microlithic porphyritic texture. The microlites consist of feldspar, albite, biotite, chlorite, and quartz. Scattered patches of leucoxene are observed, likely derived from the alteration of magmatic iron and/or titanium oxides. They are associated with areas of green chlorite, sometimes associated with actinolite, carbonate masses, and quartz. The matrix contains rare prismatic feldspar crystals with polysynthetic twinning, in addition to a multitude of actinolite prisms and partially chloritized biotite. The subhedral plagioclase microlites, which are rather stocky in shape, transform into albite, sericite, chlorite, quartz, and occasionally calcite.

Metadiorite:-

Metadiorite outcrops in blocks or slabs, often weathered, and occupies a large area of the analyzed zone (Fig. 3g). It displays a granoblastic texture characteristic of metamorphic rocks, whose mineralogical composition is dominated by plagioclase, quartz, biotite, and secondary minerals such as chlorite and calcite (Fig. 3h). Plagioclase (~ 60%) is the predominant phase of the rock and forms subhedral to euhedral crystals arranged in lamellae of varying sizes. Quartz (10-20%) appears as interstitial grains stretched between plagioclase crystals, indicating recrystallization under ductile conditions. Biotite (<10%) is generally found as inclusions in plagioclase phenocrystals, indicating crystallization prior to or concurrent with that of plagioclase. Secondary minerals, such as chlorite and calcite, are found in varying proportions and are associated with alteration processes.

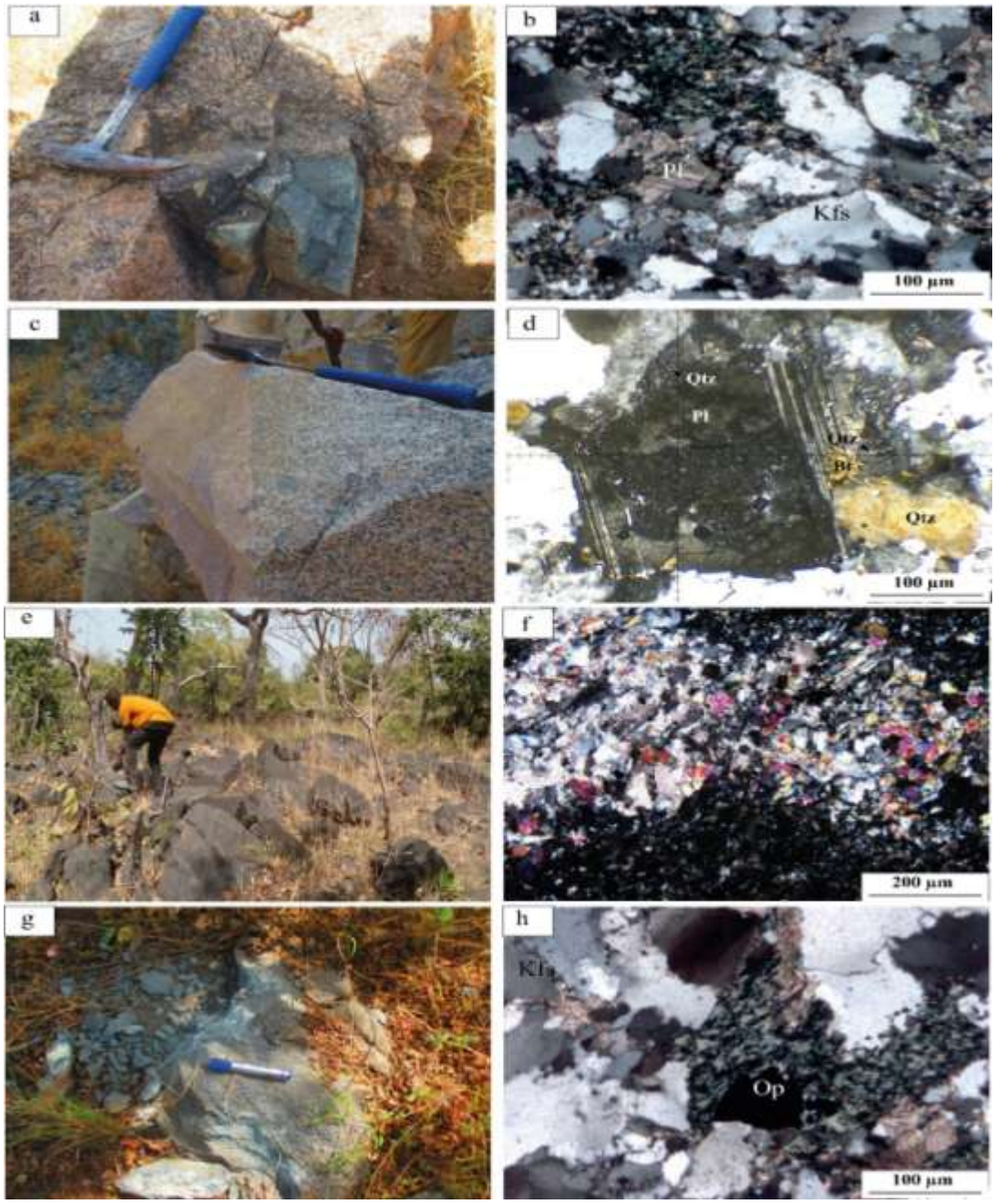


Figure 3. Photograph and microphotograph of granitoids, metagabbro, and metadiorite from the study area; a: outcrop of granodiorite enclave in granite; b: microphotograph of granodiorite; c: outcrop of granite; d: microphotograph of granite; e: outcrop of metagabbro; f: microphotograph of metagabbro; g: outcrop of metadiorite; h: microphotograph of metadiorite.

Major elements and classification:-

SiO_2 and Al_2O_3 concentrations range from 47.2% to 50.7% and 7.21% to 15.4% in the Mayo Kebbi metagabbros. These metagabbros have low alkali contents, with K_2O = 0.16% to 1.44% and Na_2O = 1.31% to 2.44%, and Fe_2O_3t (total Fe) = 7.9% to 10.1%; but low abundances of MnO (0.13% to 0.18%), TiO2 (0.44% to 0.83%), and P_2O_5 (0.01% to 0.13%), and high abundances of MgO (9.53% to 17.15%) and CaO (8.04% to 12.2%) (Table 1).

The contents of orthoclase (0.98% to 8.92%), albite (12.01% to 23.34%), anorthite (13.62% to 36.66%), olivine (6.56% to 15.87%), ilmenite (0.87% to 1.65%), magnetite (1.41% to 1.80%), apatite (0.02% to 0.30%) and hypersthene (13.23% to 20.04%) are present in the analyzed metagabbro samples. The normative differentiation index (DI = 14.26% to 37.04%) shows that the metagabbros are very poorly differentiated.

However, SiO_2 abundances in metadiorites, granite, and granodiorite range from 67.2% to 75.7%, with Al_2O_3 values ranging from 12% to 19%. These rocks have high alkali values, with K_2O = 0.86% to 3.45% and Na_2O = 4.04% to 7.54% and Fe_2O_3t (total Fe) = 0.37% to 5.06%, but low abundances of MgO (0.06% to 1.4%), MnO (0.01% to 0.16%), P2O5 (0.01% to 0.016%), CaO (1.06% to 3.12%), and TiO_2 (0.02% to 0.69%). Normative minerals such as quartz (16.19% to 35.89%), orthoclase (5.10% to 20.62%), anorthite (4.47% to 13.36%), albite (34.58% to 63.21%), hypersthene (0.55% to 8.21%), corundum (0.54% to 1.35%), magnetite (0.11% to 1.36%), ilmenite (0.04% to 1.32%), and apatite (0.02% to 0.35%) are present in the granodiorite, metadiorite, and granite samples. Some samples contain diopside at concentrations of 0.44% for CE01, 1.09% for CE11 and 0.68% for CE13. The normative differentiation index (DI = 78.63% to 91.09%) shows that the samples are highly differentiated.

Harker's diagrams (1909) show fairly clear trends for the major elements (Fig. 4). In the variation diagrams, SiO_2, Al_2O_3, CaO, Fe_2O_3, MnO, TiO_2, and P_2O_5 show linear trends with negative correlation. K2O shows limited data dispersion and a linear trend with positive correlation with SiO2. These trends probably reflect the variation in amphibole and plagioclase ratios in metamafic and granitoid rocks.

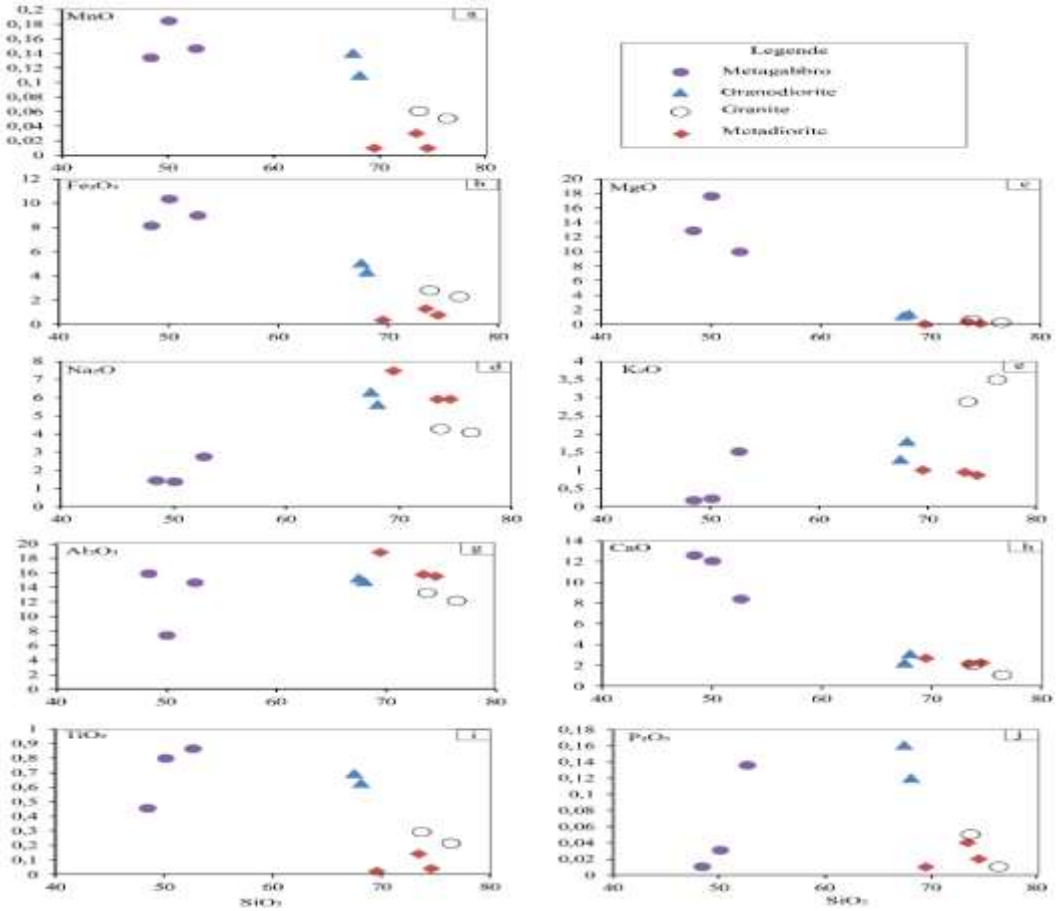


Figure 4.Haker diagram of major elements

Geochemical affinity:-

In the $Na_2O + K_2O$ vs. SiO_2 diagram (Fig. 5a:[34], the rocks in the study area belong to the subalkaline series, which allows the use of the K_2O vs. SiO_2 diagram (Fig. 5b: [34, 35]. This diagram shows that these rocks are weakly to moderately potassium-rich calc-alkaline.

In the modified alkali-lime index (MALI) vs. SiO_2 diagram[36], samples from basic enclaves, metadiorites, granodiorites, and metagabbros occupy the alkaline-calcic to calcic granite domain (Fig. 5c). Furthermore, the high alkali content (6.75-8.47%) of the rocks in the study area compared to CaO (1.06-3.12%) is characteristic of Cordillera magnesian rocks (Fig. 5d) according to the classification of[36].

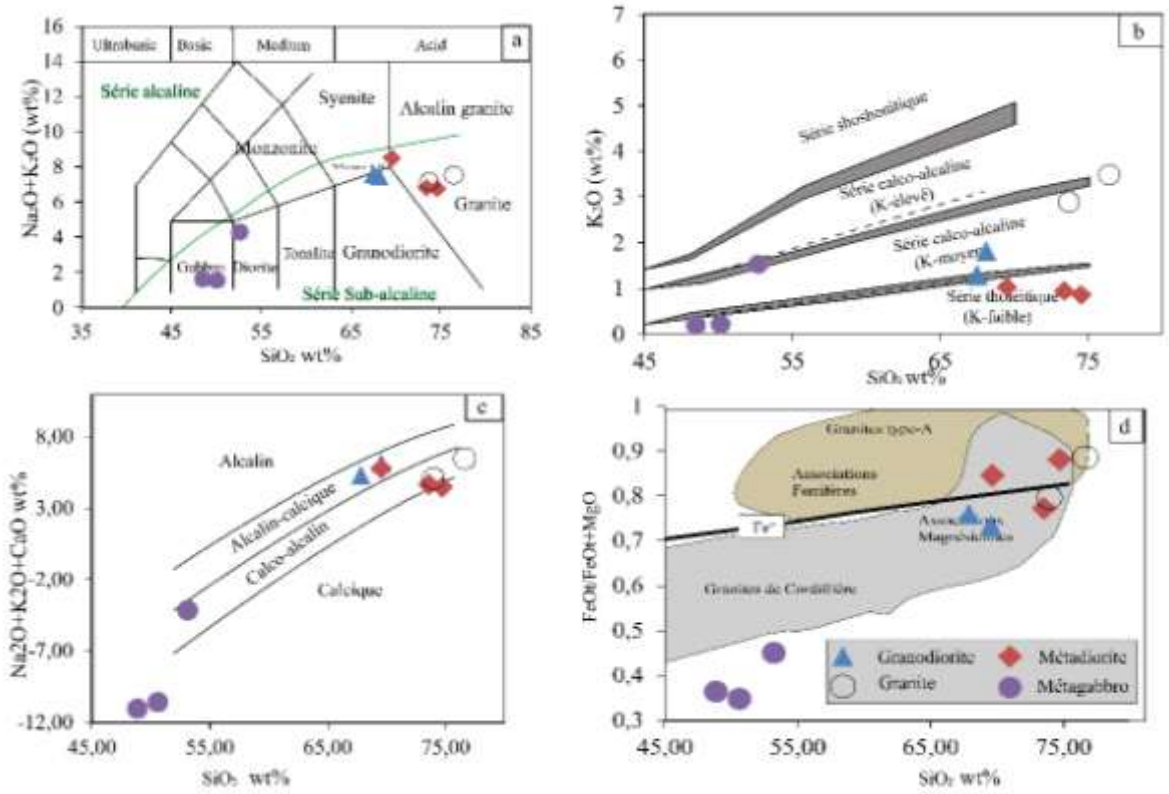


Figure 5.Geochemical affinity diagram of rocks from the study area; a: $Na_2O + K_2O$ vs. SiO_2 diagram from [34]. The boundary between the alkaline and subalkaline series is based on[37], b: K_2O vs. SiO_2 diagram. The dashed lines are from [34] and the bands arefrom [35]; c: (Na_2O+K_2O-CaO) vs. SiO_2 diagrams; d: FeOt /(FeOt + MgO) vs. SiO_2 according to[36]

Trace elements and rare earth elements:-

The analyzed samples of granodiorites, basic enclaves, metadiorites, and metagabbros (Table 1) show a slight enrichment in large ion radius elements (LILE) such as Ba (64-795 ppm), Rb (0.5-109.5 ppm) and Sr (71.9-704 ppm) compared to high-potential elements (HFSE) such as Y (2.3-159 ppm) and Nb (0.29-18.05 ppm). However, Zr exhibits high concentrations (19-268 ppm).

The diagrams in Figure 6a-b provide a clearer picture of the evolution of Rb-Sr and Sm-Nd concentrations in the granites, granodiorites, metadiorites, and metagabbros in the study area. Looking at Figure 6a, the Rb-Sr pair shows a distribution that allows the different lithological types to be distinguished; granodiorite and granite are richer in Rb and fairly rich in Sr compared to metadiorite and metagabbro. Sm-Nd contents are distributed along a positive slope, showing a continuous enrichment in Sm and Nd from metadiorite to granodiorite (Fig. 6b). Based on the work of[38],[39], and[40], the regularity of the distribution and evolution of the Sm-Nd pair is thought to be related to the stable nature of these elements during post-solidus magmatic processes.

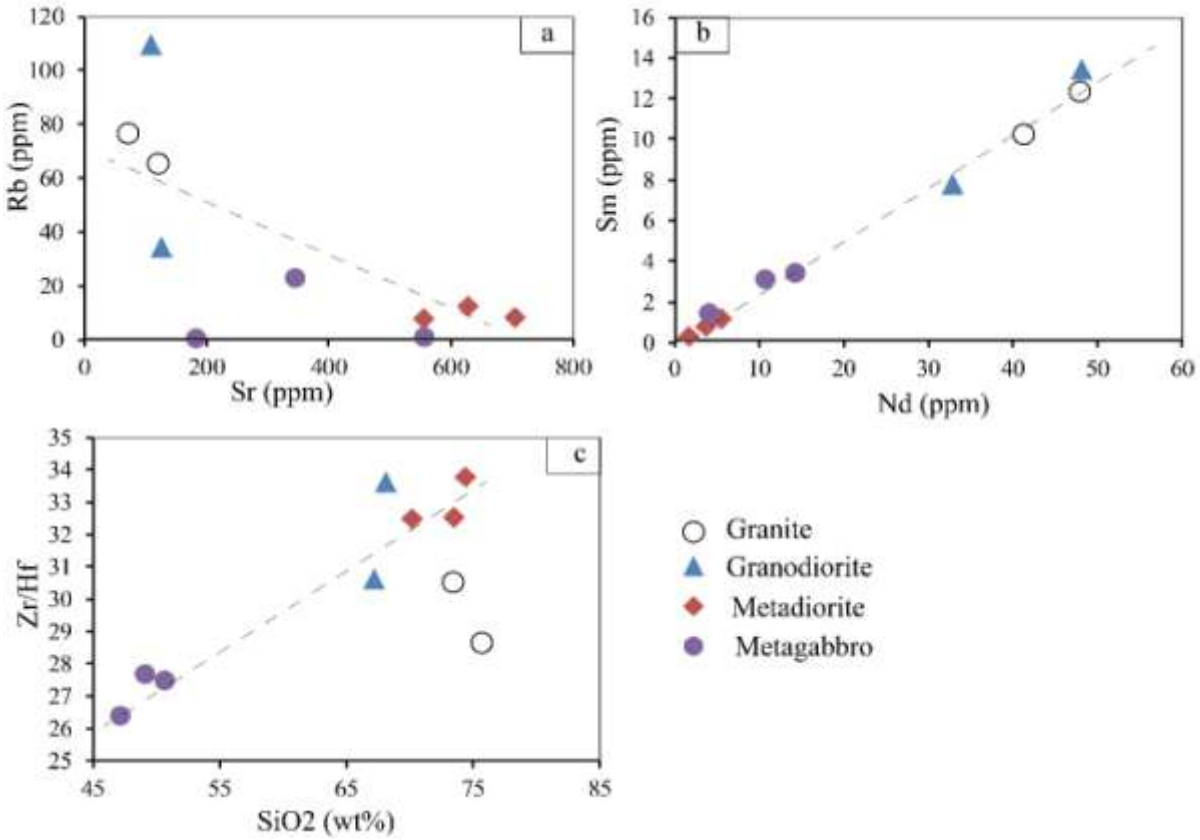


Figure 6.Evolution of trace elements and rare earth elements in granitoids, metagabbros, and metadiorites in the study area. (a, b) Evolution of Rb-Sr and Sm-Nd concentrations in granites, (c) Zr/Hf vs. SiO_2 (%) diagram.

The Zr/Hf ratio (26.38-33.75) increases from metagabbro to metadiorites (Fig. 6c; [41], reflecting an increasing fractionation index in these rocks. Furthermore, Cs concentrations (< 4.28 ppm) are low in all samples from the study area, explaining the fractional crystallization of plagioclases and magnesian minerals (Table. 1).

Table 1: Major, trace, and rare earth element concentration data for granodiorite, granite, metadiorite, and metagabbros samples from the eastern part of Mayo Kebbi.

Rock type	**Granodiorite**		**Metadiorite**			**Granite**		**Metagabbro**		
Samples	**CE01**	**CE15**	**CE19**	**CE20**	**CE21**	**CE11**	**CE13**	**CE24**	**CE27**	**CE28**
SiO2	67,2	68,1	70,2	74,4	73,5	73,4	75,7	50,7	49,1	47,2
Al2O3	15,25	14,8	19	15,45	15,75	13,2	12	14,05	7,21	15,4
Fe2O3	5,06	4,32	0,37	0,75	1,3	2,77	2,27	8,62	10,1	7,9
CaO	2,25	3,12	2,73	2,24	2,15	2,03	1,06	8,04	11,75	12,2
MgO	1,2	1,4	0,06	0,09	0,34	0,63	0,26	9,53	17,15	12,45
Na2O	6,26	5,62	7,54	5,88	5,9	4,25	4,04	2,63	1,31	1,37
K2O	1,29	1,8	1,02	0,86	0,94	2,86	3,45	1,44	0,2	0,16
Cr2O3	0,022	0,017	0,015	0,029	0,023	0,023	0,022	0,068	0,084	0,057
TiO2	0,69	0,63	0,02	0,04	0,14	0,29	0,21	0,83	0,78	0,44
MnO	0,14	0,11	0,01	0,01	0,03	0,06	0,05	0,14	0,18	0,13
P2O5	0,16	0,12	0,01	0,02	0,04	0,05	0,01	0,13	0,03	0,01
LOI	1,78	0,82	0,74	0,73	0,99	1,08	0,75	2,36	0,98	2,19
Total	99,522	100,037	100,975	99,769	100,113	99,563	99,072	96,178	97,894	97,317

Ni	6	9	<1	1	1	4	2	190	309	140
Pb	9	11	5	5	5	13	12	7	4	6
Ba	364	262	385	496	413	667	795	339	53,3	64
Cs	0,76	4,28	0,13	0,26	0,29	1,46	2,3	0,77	0,08	0,19
Ga	26,8	22,2	20,6	16,1	21,9	23,4	24,9	23,2	12,3	15,4
Hf	6,24	5,71	1,2	1,57	2,06	7,8	9,14	1,53	1,41	0,72
Nb	18,05	10,6	0,29	0,65	1,4	12,65	17,65	2,64	1,68	0,61
Rb	34,4	109,5	8	7,6	12,3	65,2	76,4	22,6	0,5	0,9
Sc	11,8	11	1,9	2,3	3,4	6,3	5	37,4	62,9	38,8
Sr	126	109,5	704	555	629	121,5	71,9	345	184,5	557
Ta	1,4	0,8	0,1	0,1	0,1	0,8	1,2	0,3	0,2	0,1
Th	4,82	6,06	0,18	0,08	0,24	5,68	6,74	0,19	0,06	0,09
Ti	0,43	0,39	0,01	0,03	0,09	0,17	0,13	0,53	0,49	0,28
U	1,94	2,36	0,14	0,05	0,06	1,4	1,58	0,16	<0.05	<0.05
V	74	77	<5	7	13	26	13	227	216	128
Y	159	56,1	2,3	2,9	3,3	75,2	96,1	18,4	17,2	8
Zr	191	192	39	53	67	238	262	42	39	19
La	27,7	27,3	3,8	1,6	4,7	31,5	36,4	7,4	3,7	1,8
Ce	52,3	49,8	6,2	2,8	10,2	71	87,6	17,2	11,8	4,9
Pr	10,05	7,85	0,92	0,39	1,26	9,38	10,9	2,95	1,95	0,81
Nd	48,1	32,8	3,7	1,7	5,6	41,3	47,8	14,4	10,8	4,2
Sm	13,45	7,78	0,78	0,33	1,18	10,25	12,35	3,4	3,13	1,45
Eu	2,85	1,86	0,34	0,26	0,36	1,53	1,86	1,12	0,84	0,55
Gd	18,65	8,4	0,58	0,4	0,88	12,25	14,1	3,47	3,08	1,56
Tb	3,27	1,44	0,08	0,08	0,12	2,18	2,5	0,53	0,55	0,25
Dy	22,1	9,14	0,42	0,44	0,65	13,1	16,05	2,96	3,04	1,62
Ho	4,92	1,88	0,08	0,09	0,11	2,71	3,35	0,62	0,64	0,31
Er	15,1	5,58	0,24	0,28	0,27	8,04	10,5	1,74	1,85	0,91
Tm	2,3	0,9	0,04	0,06	0,04	1,17	1,62	0,26	0,26	0,12
Yb	13,25	5,81	0,21	0,36	0,24	7,43	10,4	1,52	1,54	0,72
Lu	2,16	0,92	0,04	0,06	0,03	1,16	1,6	0,23	0,22	0,11
Zr/Hf	30,61	33,63	32,50	33,76	32,52	30,51	28,67	27,45	27,66	26,39
Nb+Y	177,05	66,70	2,59	3,55	4,70	87,85	113,75	21,04	18,88	8,61
La/Sm	2,06	3,51	4,87	4,85	3,98	3,07	2,95	2,18	1,18	1,24
LREE	506,62	405,36	49,42	21,47	70,27	509,44	601,98	145,55	100,65	43,30
HREE	721,84	298,48	14,35	16,51	18,42	415,75	527,55	95,69	95,38	46,51
La/Lu	1,33	3,08	9,86	2,76	16,26	2,81	2,36	3,33	1,74	1,69
La/Sm	1,28	2,19	3,04	3,02	2,48	1,91	1,84	1,35	0,73	0,77
Gd/Lu	1,06	1,12	1,79	0,82	3,62	1,30	1,08	1,86	1,73	1,75
Eu/Eu*	0,54	0,70	1,54	2,18	1,07	0,41	0,42	0,99	0,82	1,11

The rock spectra of the Bagaroua-Fianga massifs are heterogeneous (Fig. 7) and characterized by low fractionation (i) [(La/Lu)N = 1.33–3.08] of LREE [(La/Sm)N = 1.28 - 2.19] compared to HREE [(Gd/Lu)N = 1.06-2.12] in granodiorite (Fig. 7a), (ii) moderate [(La/Lu)N = 2.36 - 2.81] of LREE [(La/Sm)N = 1.84 - 1.91] compared to HREE [(Gd/Lu)N = 1.08 - 1.30] in granite (Fig. 7b), (iii) moderate [(La/Lu) N = 2.76–16.26] of LREE [(La/Sm)N = 2.48–3.04] compared to HREE [(Gd/Lu)N = 0.82–3.62] in metadiorite (Fig. 7c) and (iv) moderate [(La/Lu) N = 1.69–3.33] of LREE [(La/Sm)N = 0.73–1.35] relative to HREE [(Gd/Lu)N = 1.73–1.86] in the metagabbro (Fig. 7d). The granodiorites show pronounced negative anomalies in Eu (Fig. 7a) with δEu = 0.54–0.70 (Table 1).

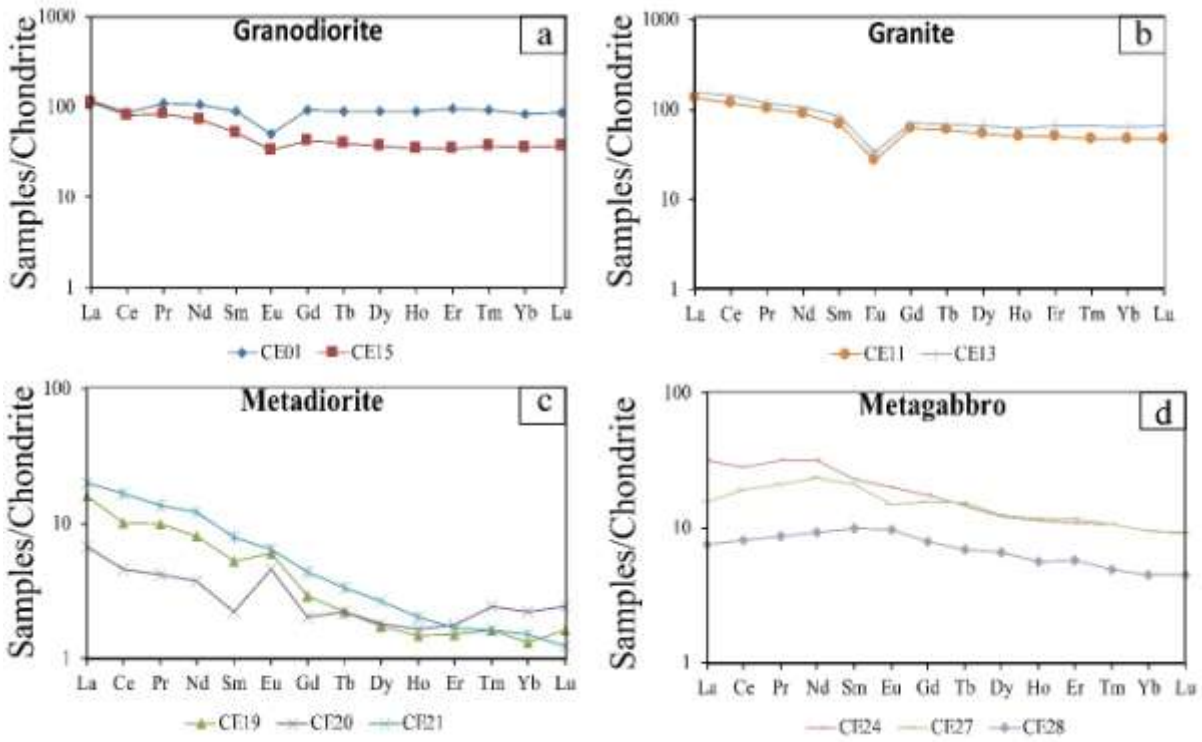


Figure 7.Rare earth spectra of granites from the study area. Normalized to[42] chondrite values.

The contents of certain trace elements in the study area are normalized to[43] primitive mantle average values. The spidergrams in Figure 8 reveal a strong enrichment in the most incompatible elements (Cs, Ba, Rb, Th, U, etc.) compared to the least incompatible elements (Y, Ho, Er, Tm, Yb, etc.), with negative anomalies in Th, Nb, Sm, Sr, Zr, and Ti and positive anomalies in Ba, Th, U, K, Hf, and Gd, which are characteristic features of calc-alkaline magmas in orogenic zones and the continental crust in general[44, 45, 46]. In detail, fundamental variations appear between the spidergrams of the different rocks in the study area. The spidergrams for these granitoids show a pronounced negative anomaly in Ti (Fig. 8a), except in the metagabbros (Fig. 8d). In the metadiorite and metagabbro, the profile shows a negative anomaly in P and a positive anomaly in Sr (Fig. 8c, d). Furthermore, the negative anomaly in Ba in the granites (Fig. 8a) suggests that fractional crystallization of potassium feldspars and biotite was very significant during the formation of these rocks.

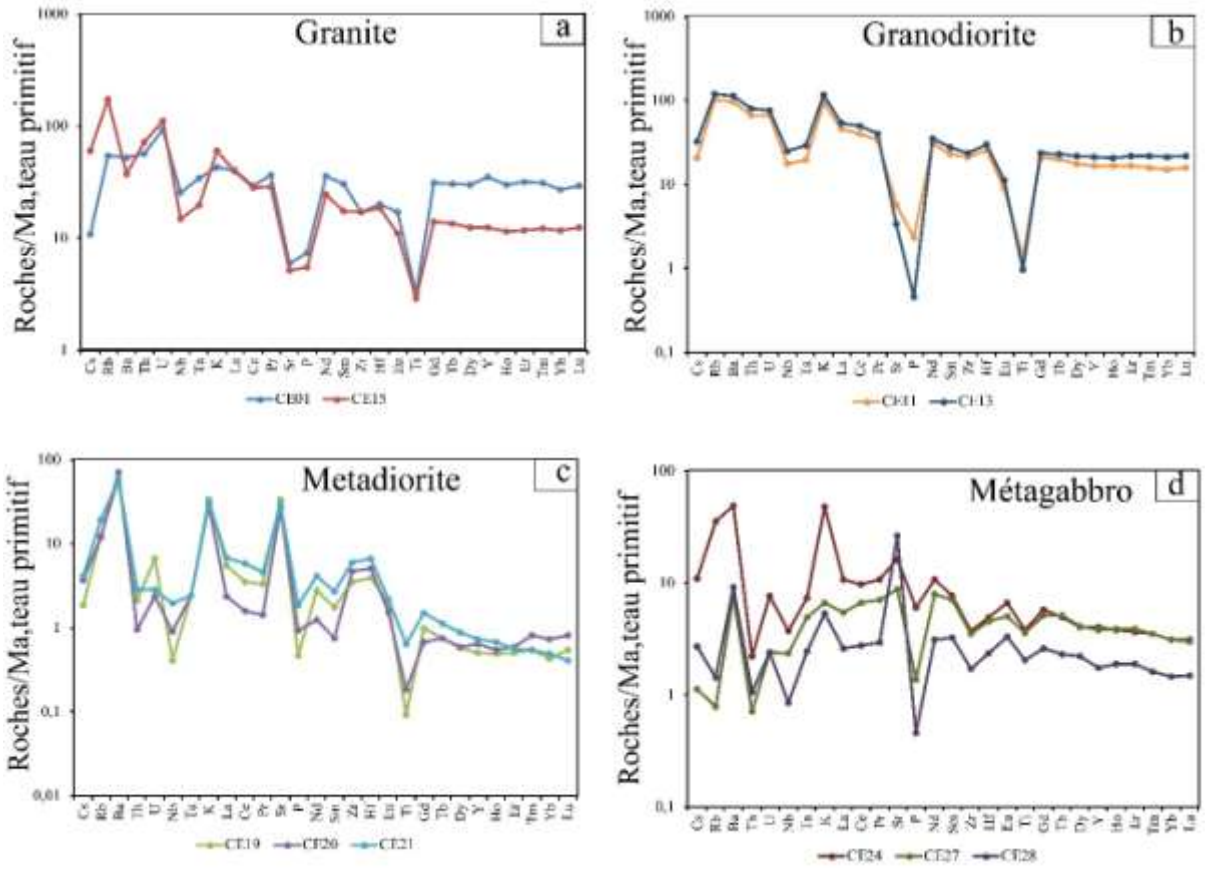


Figure 8.Spider diagrams of trace elements in granitoids from the study area. Normalization relative to the primitive mantleof [43].

The spectra of granitoids in the study area are homogeneous and characterized by significant fractionation (i) [(La/Lu)N = 1.38-16.87] of LREE [(La/Sm)N = 0.76-3.13] relative to HREE [(Gd/Lu)N = 0.82-3.64].

Discussion:-

Nature of the rocks:-

The rocks in the study area are calc-alkaline to calcic, moderately potassic, and magnesian. The granite and granodiorite (A/CNK = 0.30-1.08) are metaluminous to peraluminous. Metadiorite (A/CNK = 1.03 and 1.08) is peraluminous, while metagabbro (A/CNK = 0.30-0.69) is essentially metaluminous. Metadiorite (A/CNK = 1.03 and 1.08) has the characteristics of S-type granitoids according to the classification of [47] and [48]. Furthermore, in the Pb vs. SiO2 diagrams (Fig. 9a), Pb abundances increase with rising SiO_2 contents in granitoids and metadiorites, following the respective trends for type I and S granites proposed by[49] and[47]. In the Na_2O vs. K_2O discrimination diagram (Fig. 9b:[48,50]), granodiorite and metadiorite are type I. In contrast, all of the metagabbro and granite analyzed are restricted to the field of type S rocks. In general, this diagram shows that the most sodic samples exhibit a relationship to type-I rocks, while the least sodic samples have an affinity for type-S rocks.

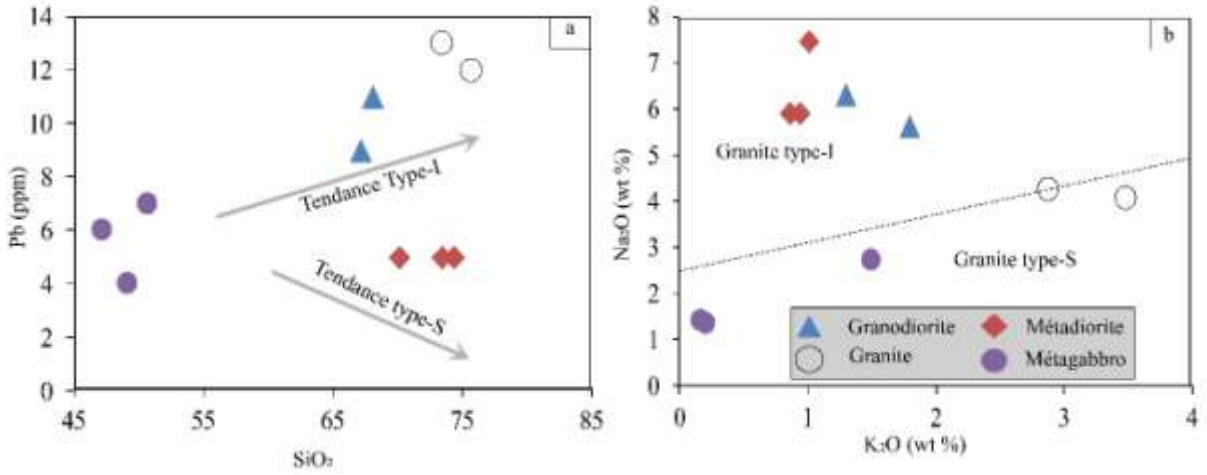


Figure 9. Genetic relationship between granitoids and metadiorites and metagabbros in the study area. (a) Pb vs. SiO2 diagrams with evolution vectors for type-I and -S granites [47, 49], (b) Na2O vs. K2O diagram[48,50].

Source of granitic magmas:-

The metaluminous to peraluminous nature of the rocks analyzed suggests a source consisting of immature plutonic materials or metaluminous basaltic to andesitic rocks [51, 52]. However, such basaltic to andesitic metaluminous rocks generally show enrichment in Na_2O and Sr [53] and K_2O/Na_2O ratios < 1 [54], which contrasts significantly with the granodiorites and metaluminous granites in this study, for which the Sr (71.9-126 ppm, mostly < 150 ppm) and Na_2O (4.04-6.26%) contents are low and the K_2O/Na_2O ratios (0.20-0.85) are < 1.

There is considerable evidence to suggest that the peraluminous granites and granodiorites in the study area derive mainly from a continental source comprising metasediments under supracrustal conditions: (i) they exhibit low Mg-number values (Mg# = 0.26-1.39), high SiO2 (67.52-76.40%), K2O (1.29-3.48%) contents and A/CNK ratios (0.96-1.08), suggesting essentially a crustal source through meta-igneous protoliths [55, 56]; (ii) their weakly fractionated HREE spectra [(Gd/Lu) N = 0.82-3.64] and very low Sr/Y ratios (0.74-1.95) indicate that the peraluminous granites and granodiorites in the study area derive from a relatively shallow crustal source above the garnet stability depth [57, 58]and (iii) these granites and granodiorites are more enriched in Rb, Th, K, Nb-Ta, Nd and more depleted in Sr, P, Ti (Fig. 8d) than the upper continental crust, indicating that their source was more felsic than typical supracrustal magmas [59].

Fractional crystallization:-

Harker diagrams and distribution patterns of the major elements MgO, Fe_2O_3, and MnO with SiO_2 indicate fractional crystallization of clinopyroxene and hornblende. Furthermore, in the La/Sm and $(La/Yb)_N$ vs. La diagrams (Fig. 10a-b;)[60], the Bagaroua-Fianga granitoids in Mayo Kebbi also align with the fractional crystallization trajectory. Negative correlations between SiO_2 and MgO, CaO, TiO_2, Fe_2O_3 indicate fractionation dominated by ferromagnesian phases (biotite, amphibole: Fig. 4), while elements (e.g., TiO_2 and P_2O_5) inversely correlated with SiO_2 suggest fractionation of accessory minerals (apatite, titanite, zircon, monazite).

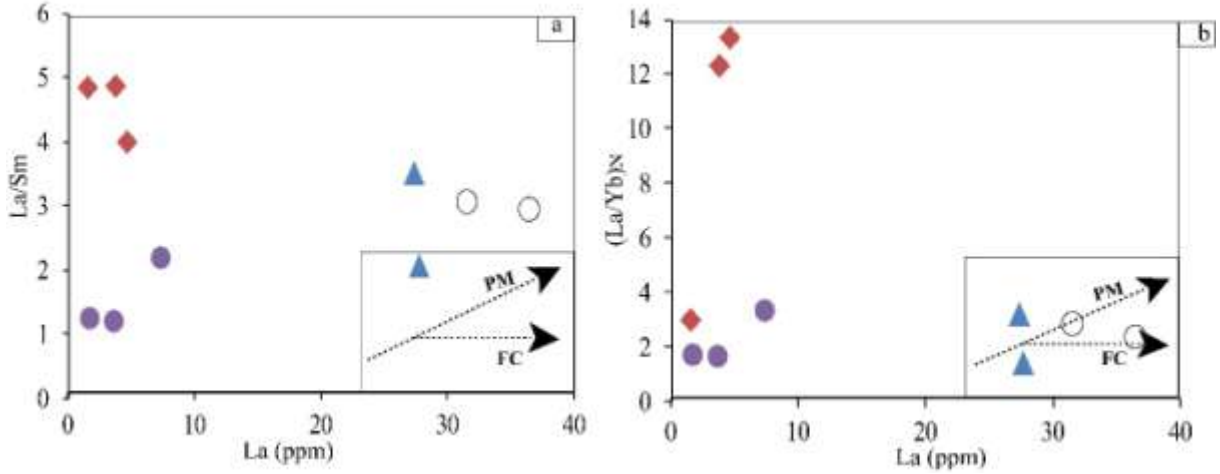


Figure 10. Evolution process of Mayo Kebbi granitoids. Diagrams (a-b) La/Sm and $(La/Yb)_N$ vs. La [60]defining the trajectories of fractional crystallization (FC) and partial melting (PM).

The enrichment in LREE relative to HREE (La_N/Yb_N varying between 1.42–3.19) and the flat profile (Dy_N/Yb_N varying between 0.80–1.31) of HREE in the rocks of the Bagaroua-Fianga massif lead us to propose that these rocks originate from fractional crystallization of mantle rocks [61].

Geodynamic context:-

Structural observations in the field reveal a NS to NE-SW oriented hill formation of metadiorites and metagabbros. This arrangement is identified in the Bagaroua-Fianga granitoids and is similar to those described in the syn-folding granitoids of southern Chad, such as the Baïbokoum syenitic pluton[15], the Guider granitoids in northern Cameroon [62], the Ouaddaï granodiorite [10], the Bitkine gabbro-diorites in Guéra[63] and the post-collisional granitic complex in western Cameroon[64]. Furthermore, using the tectonic diagram by[65], these diorites from Guider, Ouaddaï, Guéra de Baïbokoum, and Mayo Kebbi were interpreted as syn-subduction alkaline rocks. In this same diagram [Zr-Ce-Sm-Y-Yb]NYTS vs. [Rb-Th-U-Ta] NYTS[65], the granites, granodiorites, metagabbros, and metadiorites of the study area also occupy the domain of strongly potassic calc-alkaline granitoids (CAFP), which is that of syn- to post-collisional syn-shearing granitoids (Fig. 11).

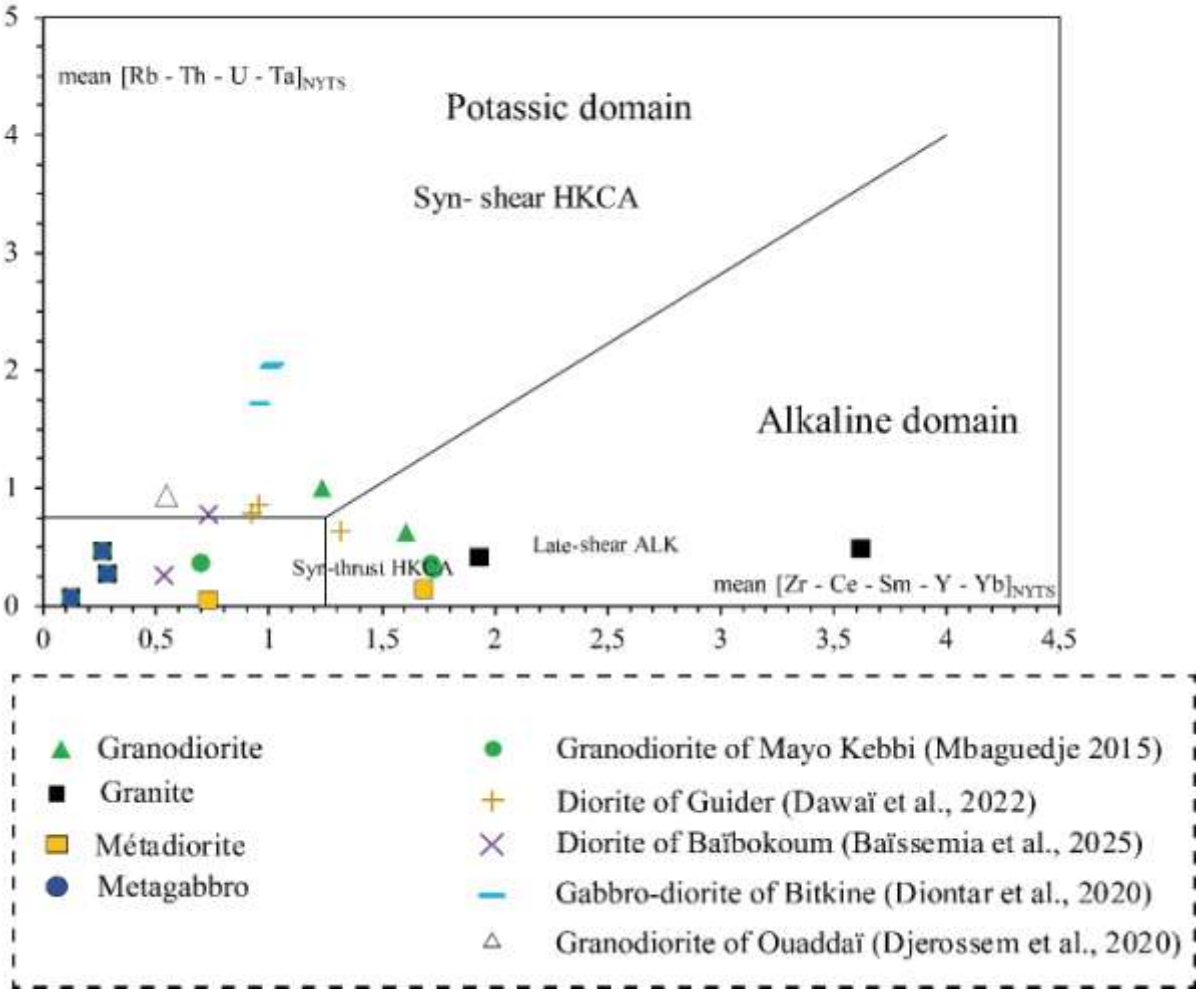


Figure 11.SNY vs. SNX diagram for granitoids and mafic rocks from Mayo Kebbi. Comparison with the composition of granodiorites, diorite, and gabbro-diorite from Mayo Kebbi [33], Guider [62], rocks from the Baïbokoum pluton [15], Ouaddaï[10] and the Bitkine massif [63]. SNY = mean [Rb-U-Th-Ta]NYTS; SNX = mean [Zr-Ce-Sm-YYb]NYTS. NYTS = normalization to the Yenchichi-Telabit series [65].

The Mayo Kebbi massif is composed of calc-alkaline granitoids with low to medium potassium content and exhibits a volcanic arc geochemical signature [66]Fig. 12. However, a magnesian series reflects an affinity with relatively hydrated and oxidizing magmas and source regions[67], which corresponds to origins largely linked to subduction. Low-potassium calc-alkaline magmatism is widespread in post-collisional stages [65, 68], but it also occurs at active continental margins [68, 69]. Furthermore, the granitoids of the Mayo Kebbi massif formed in a post-orogenic tectonic environment. Post-orogenic extension is always triggered by the delamination of the subducted plate [64, 70].

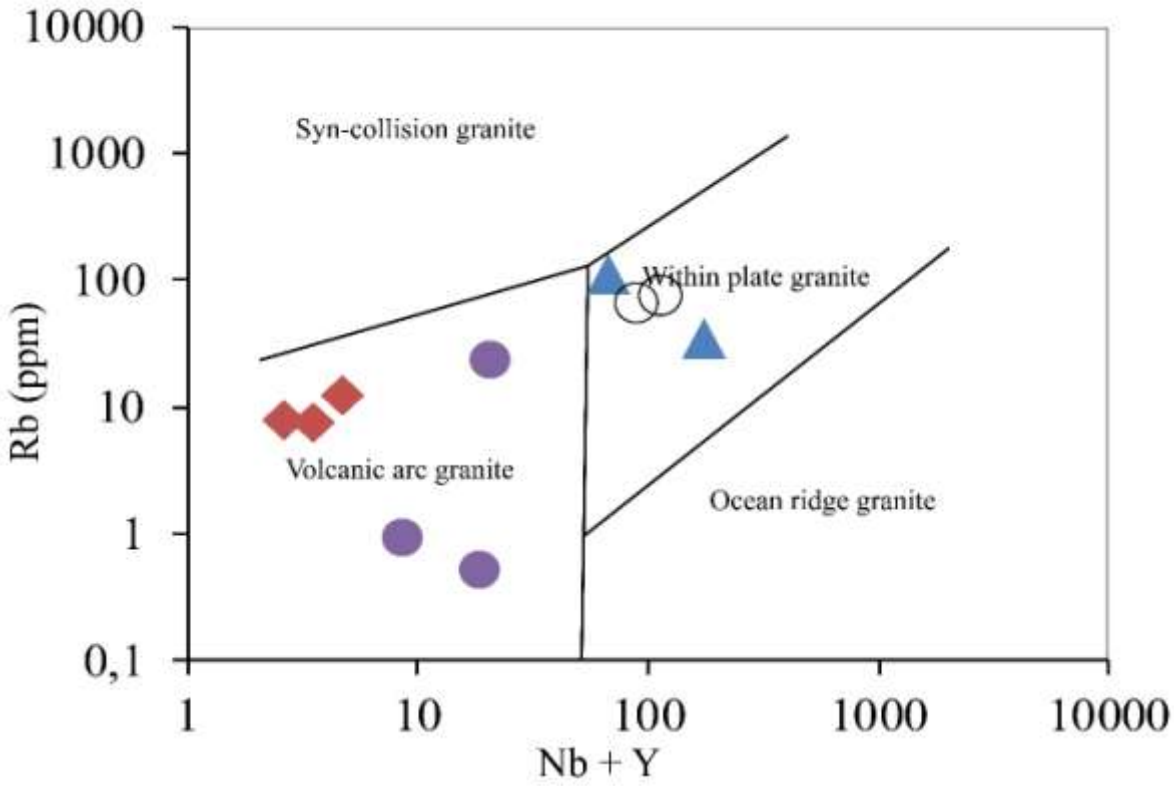


Figure 12. Tectonic discrimination diagram[66].

Conclusion:-

Based on field and petrographic data collected on the Bagaroua-Fianga massif in Mayo Kebbi, four rock categories have been identified: granodiorite, granite, metadiorite, and metagabbro. The predominant mineral phases in these rocks include alkali feldspar, quartz, plagioclase, clinopyroxene, and biotite in smaller quantities, as well as apatite, zircon, and various accessory opaque minerals. Geochemical data for the whole rock indicate a subalkaline affinity to the rocks of the Mayo Kebbi massif, which is part of the calc-alkaline to shoshonitic series with average K content. The field, petrographic, and geochemical evidence presented here suggests that fractional crystallization and magma interpenetration mechanisms may be more significant for understanding the origin of the granites and granodiorites of the Mayo Kebbi massif, which may have resulted from the melting of metagabbros. Nevertheless, the rocks of the massif appear to have been established in a post-collisional setting. Their magmas possess the characteristics of a mantle source altered by subduction material. This transformed source would have undergone partial melting during the lithospheric delamination of the post-collisional phase of the Pan-African orogenic cycle in Chad.

Acknowledgements:-

This study is part of a larger scientific research project led by the first author. The authors express their deep gratitude to the administrative authorities of Pala for their invaluable assistance and for granting permission to conduct fieldwork in this region. They extend special thanks to Mr. Che Stephene (Douala) for his essential technical support during the sample pulverization process. The authors also wish to express their deep gratitude to the team at ALS Geochemistry, based in Loughrea, Ireland, whose expertise and dedication were crucial to the completion of the geochemical analyses.

Declaration:-

Conflicts of interest:-

The authors declare that they have no competing financial interests or known personal relationships that could influence the work presented in this article.

References:-

1. Bessoles, B. & Trompette, R. (1980). La chaîne Pan-Africaine zone mobile d'Afrique centrale (partie sud) et zone mobile soudanaise. Mémoire B.R.G.M. 92, 326 p.
2. Abdelsalam, M., Liégeois, J.-P. & Stern, R. J. (2002). The Saharan Metacraton. Journal of African Earth Sciences, 34, 119-136. http://dx.doi.org/10.1016/S0899-5362(02)00013-1
3. Ganade de Araujo, C. E., Weinberg, R. F. &Cordani, U.G. (2014).Extruding the Borborema Province (NE-Brazil): a two-stage Neoproterozoic collision process, Terra Nova, 26, 157-168. https://doi.org/10.1111/ter.12084.
4. Ganade Carlos E., Weinberg Roberto, F., Caxito Fabricio, A., Lopes Leonardo, B. L., Tesser Lucas, R. & Costa Iago, S. (2021). Decratonization by rifting enables orogenic reworking and transcurrent dispersal of old terranes in NE Brazil. Nature. Scientific Reports 11:5719 https://doi.org/10.1038/s41598-021-84703-x
5. Lino, L. M., Quiroz-Valle F. R., Basei, MÂS, Vlach, S. R. F., Hueck, M., Willbold, M. & Lemos-Santos, D. V. (2023). Petrogenesis and tectonic significance of two bimodal volcanic stages from the Ediacaran Campo Alegre-Corupá Basin (Brazil): Record of metacratonization during the consolidation of Western Gondwana. Precambr Res 385:106950
6. Ngako, V., Affaton, P., Nnange, J. M. & Njanko, T. (2003). Pan-African tectonic evolution in central and southern Cameroon: transpression and transtension during sinistral shear movements. Journal of African Earth Sciences, 36, 207-214.
7. Ferré E., Gleizes G. & Caby, R. (2002). Obliquely convergent tectonics and granite emplacement in the Trans-Saharan belt of Eastern Nigeria: a synthesis. Precambrian Research 114:199–219.
8. Suayah, I. B., Miller, J. S., Miller, B. V., Bayer, T. M. and Rogers, J. J. (2006). Tectonic significance of late Neoproterozoic granites from the Tibesti massif in southern Libya inferred from Sr and Nd isotopes and U-Pb zircon data. Journal of African Earth Sciences 44:561–570.
9. Kasser, M.-Y. (1995).Evolution précambrienne de la région du Mayo- Kebbi (Tchad).Un segment de la chaîne panafricaine. Thèse Muséum National d'Histoire Naturelle de Paris, 217p.
10. Djerossem, N. F., Berger, J., Vanderhaeghe, O., Isseini, M., Ganne, J. & Zeh, A. (2020). Neoproterozoic magmatic evolution of the southern Ouaddaï Massif (Chad). Bulletin de la Société Geologique de France (BSGF) 191:34
11. Djerossem, N. F., Zeh, A., Isseini, M., Vanderhaeghe, O., Berger, J. & Ganne, J. (2021). U-Pb-Hf isotopic systematics of zircons from granites and metasediments of southern Ouaddaï (Chad), implications for crustal evolution and provenance in the Central Africa Orogenic Belt. Precambrian Research 361:106233.
12. Djerossem, N. F., Mbassa, J. B., Vanderhaeghe, O. & Gregoire, M. (2024). The Iriba alkaline basalts, an expression of mantle derived Cretaceous magmatism of the Cameroon-Chad volcanic line along the Central Africa Rift System. Comptes Rendus. Geoscience-Sciences de la Planete 356 :231-248
13. De Wit, M. J., Bowring S., Buchwaldt, R., Dudas F. Ö., MacPhee, D., Tagne-Kamga, G., Dunn, N., Salet, A.M. &Nambatingar, D. (2021). Geochemical reconnaissance of the Guéra and Ouaddaï Massifs in Chad: evolution of Proterozoic crust in the Central Sahara Shield. South African Journal of Geology 124:353-382.
14. Shellnutt, J. G., Denyszyn, S. W. & Pang, K. N. (2021). Editorial: Granite Petrogenesis and Geodynamics. Frontiers in Earth Sciences 8:637729.
15. Baïssemia, R. G., Gountié, D. M., Tcheumenak, K. J., Klamadji, N. M., Mbaguedjé, D. & Kwékam, M. (2025). Petrography and geochemical characterization of the Baïbokoum syenitic pluton (Southern Chad): implication for the magma genesis. Acta Geoch. 44(2), 420-439. https://doi.org/10.1007/s11631-024-00733-y
16. Ronang Gustave Baïssemia, Diondoh Mbaguedjé, Nenadji Félix Djerossem, Ousmanou Safianou, Nourene Souleymane Abdoulaye, Dedzo Merlin Gountié, Maurice Kwékam (2025). Incorporation of Geospatial Data and Multi-Criteria Analysis for Mapping and Assessing the Mineral Potential of the Baïbokoum Pluton (Southern Chad),Open Journal of Geology, 2025, 15(12), 1029-1060,https://www.scirp.org/journal/ojg
17. Isseini, M. (2011).Croissance et différenciation crustales au Néoprotérozoïque: Exemple du domaine panafricain du Mayo Kebbi au Sud-Ouest du Tchad(Doctoral dissertation, Université Henri Poincaré-Nancy 1).
18. Isseini, M, André-Mayer, A., Vanderhaeghe, O., Barbey, P. & Deloule, E. (2012). A-type granites from the Pan-African orogenic belt in South-Western Chad constrained using geochemistry, Sr-Nd isotopes and U-Pb geochronology. Lithos 153:39–52
19. Poidevin, J. L. (1991). Les ceintures de roches vertes de la République Centrafricaine. Contribution à la connaissance du Précambrien du nord du craton du Congo. Doctorat d'Etat, Université Blaise Pascal, Clermont-Ferrand (France), 208p.
20. Rolin P. (1995). La zone de décrochements panafricains des Oubanguides en République Centrafricaine. Comptes Rendu De L'académie Des Sciences De Paris 320:63–69 (in French)

21. Toteu, S. F., Van Schmus, W. R., Penaye, J. &Michard, A. (2001). New U-Pb and Sm-Nd data from north-central Cameroon and its bearing on the pre-Pan African history of central Africa. Precambrian Research, 108, 45–73.
22. Toteu, S. F., Penaye, J. & Poudjom, D. Y. (2004). Geodynamic Evolution of the Pan-African Belt in Central Africa with Special Reference to Cameroon. Canadian Journal of Earth Sciences, 41, 73-85.
23. Toteu, S. F., Penaye, J., Deloule, E., Van Schmus, W. R. &Tchameni, R. (2006). Diachronous evolution of volcano-sedimentary basins north of the Congo craton: insights from UPb ion microprobe dating of zircons from the Poli, Lom and Yaoundé groups (Cameroon). Journal of African Earth Sciences, 44, 428–442.
24. Ngako, V. (1999). Les Déformations continentales Pan-Africaines en Afrique Centrale. Résultat d'un poinçonnement de type himalayen. [State Thesis, University of Yaoundé I], 301p.
25. Njonfang, E., Ngako V., Kwekam M., & Affaton P. (2006). Les orthogneissCalco-Alcalins de Foumban–Bankim: Témoins d'une zone interne de Marge active Panafricaine En Cisaillement. C R Geosciences 338(9):606–616 (in French)
26. Tchakounté, J., Eglinger, A., Toteu, S.F., Zeh, A., Nkoumbou, C., Mvondo, O.J., Penaye, J., De Wit, M. and Barbey, P. (2017) The AdamawaYadé domain, a piece of archaean crust in the neoproterozoic central African orogenic belt (Bafia area, Cameroon). Precambrian Res 299:2010–2229
27. Klamadji Moussa Ngarena, Tekoum Léotine, Baïssemia Ronang Gustave, Merlin Gountié Dedzo, Djérossem Nenadji Felix, Béninga Léopold Felix & Didi Djamilatou (2025) Geochemical Characterizations of the Hypovolcanic Formations of the Pan-African Basement and the Cretaceous Sedimentary Basins of Figuil (North Cameroon) and Léré (South-West Chad): Petrogenetic and Geodynamic Implication of the Pan-African Range of Central Africa (CPAC), International Journal of Geosciences, 2025, 16(2), 127-153https://www.scirp.org/journal/ijg
28. Mbaguedje Diondoh, Félix Nenadji Djerossem, Gustave Ronang Baïssemia, Moussa Ngarena Klamadji (2025) Petrographic and Geochemical Characterization of Metaluminous to Peraluminous Granitoids from Goueygoudoum-Fianga (Southwestern Chad): Insights into Magma Sources and Tectonic Setting, Open Journal of Geology, 2025, 15(11), 826-848, https://www.scirp.org/journal/ojg
29. Félix Nenadji Djerossem, Gustave Ronang Baïssemia, Moussa Ngarena Klamadji, Mbaguedje Diondoh3 (2025) Petrogenesis and Tectonic Significance of Meta-Mafic Rocks from Eastern Mayo Kebbi Massif (Pala), Chad: Evidence for a Depleted Mantle Source and Intra-Oceanic Subduction, International Journal of Geosciences, 2025, 16(10), 701-721, https://www.scirp.org/journal/ijg
30. Felix Nenadji Djerossem, Jean Wanloana Djobelao and Gustave Ronang Baissemia (2026) Petrography and geochemical characterization of the lame alkaline basalts (southwestern mayo kebbi) in the cameroonchad volcanic line: implications for tectonic evolution and mantle source, International Journal of Advanced Research (IJAR) Article DOI:10.21474/IJAR01/22762, DOI URL:http://dx.doi.org/10.21474/IJAR01/22762
31. Bouyo Houketchang, M., Zhao, Y., Penaye, J., Zhanga, S. H. & Njelb, U. O. (2015). Neoproterozoic subduction-related metavolcanic and metasedimentary rocks from the Rey Bouba Greenstone Belt of north-central Cameroon in the Central African Fold Belt: New insights into a continental arc geodynamic setting. Precambrian Research, 261, 40- 53.
32. Pouclet, A., Vidal, M., Doumnang, J.-C., Vicat, J. P. & Tchameni, R. (2006). Neoproterozoic crustal evolution in Southern Chad: Pan-African ocean basin closing, arc accretion and late- to post-orogenic granitic intrusion. Journal of African Earth Sciences, 44, 543-560. http:/dx.doi.org/10.1016/j.jafrearsci.2005.11.019
33. Mbagdje, D. (2015). Métallogénie de l'or et de l'uranium dans le cadre de la croissance et de la différenciation de la croûte au Néoprotérozoïque : Exemple du massif du Mayo-Kebbi (Tchad) dans la Ceinture Orogénique d'Afrique Centrale. Thèse de Doctorat, Université de Lorraine, France, 270pp
34. Le Maître, R. W., Bateman, P., Dubek, A., Keller, J., Lameyre, J., Le Bas, M. J., Sabine, P. A., Schmid, R., Sorensen, H., Streckeinsen, A., Woolley, A.R. & Zanettin, B. (1989). A classification of igneous rocks and glossary of terms. Recommendations of the International Union of Geological Sciences Subcommission on the Systematics of Igneous Rocks. Blackwell, Oxford, 193p
35. Rickwood, P.C. (1989). Boundary lines within petrologic diagrams which use oxides of major and minor elements. Lithos, 22, 247-264.
36. Frost, B. R., Barnes, C. G., Collins, W. J., Arculus, R.J., Ellis, D. J. & Frost, C. D. (2001) A geochemical classification for granitic rocks. Journal of Petrology, 42, 2033-2048. http://dx.doi.org/10.1093/petrology/42.11.2033
37. Irvine, T.N. & Baragar, W.R.A. (1971). A guide to the chemical classification of the common volcanic rocks. Canadian Journal of Earth Sciences, 8, 523-548.

38. Ben Othman, D., Fourcade, S. & Allègre, C. J. (1984). Recycling processus in granitegranodiorite complex genesis: The Querigut case studied by Nd-Sr isotope systematics. Earth and Planetary Sciences Letters, 69, 290-300.
39. Davidson, J. P., da Silva, S. L., Holden, P. & Halliday, A.N. (1990). Small-scale desequilibrium in a magmatic inclusion an its more silicic host. Journal of Geophysical Research, 95, 17661-17675.
40. Roberts, M. P., Pin, C., Clemens, J. D. & Paquette, J. L. (2000). Petrogenesis of mafic to felsic plutonic rock associations: The Calc-alkaline Quérigut Complex, French Pyrénées. Journal of Petrology, 41 (6), 809-844.
41. Mc Donough, W. F. &Sun, S. S. (1995). The Composition of the Earth. Chemical Geology, 120, 223-253.
42. Sun, S. S. & McDonough, W.F. (1989). Chemical and isotopic systematics of oceanic basalts: implications for mantle composition and processes. Geological Society of London, Special Publication, 42 (1), 313-345.
43. Saunders, A. D., Tarney, J., & Weaver, S. D. (1980). Transverse geochemical variations across the Antarctic Peninsula: implications for the genesis of calc-alkaline magmas. Earth and Planetary Sciences Letters, 46, 344-360.
44. Thompson, R. N., Morrison, M. A., Hendry, G. L., & Parry, S. J. (1984). An assessment of the relative role of crust and mantle in magma genesis: An elemental approach. Philosophia, Transactions of the Royal Society, London, 310, 549-590.
45. Taylor, S. R. & McLennan, S.M. (1985). The continental crust: Its composition and evolution. Oxford, United Kingdom, Blackwell Scientific Publication, 312p.
46. Chappell, B. W. (1999). Aluminium saturation in I- and S-type granites and the characterization of fractionated haplogranites. Lithos, 46, 535-551.
47. Chappell, B. W. & White, A. J. R. (2001). Two contrasting granite types: 25 years later. Australian Journal of Earth Sciences, 48, 489-499.
48. Chappell, B. W. & White, A. J. R. (1992). I-and S-type granites in the Lachlan Fold Belt. Transition of the Royal Society Edinburgh: Earth Science, 83,1-26. http://dx.doi.org/10.1017/S0263593300007720
49. Chappell, B.W. &White, A. J. R. (1984). I- and S-type granites in the Lachlan Fold Belt, southeastern Australia. In Xu Keqin and Tu Guangchi (Eds.), Geology of granites and their metallogenic relations (pp. 87-101). Beijing Scientific Press.
50. Clemens, J. D., Stevens, G. & Farina, F. (2011). The enigmatic sources of I-type granites: the peritectic connexion. Lithos, 126, 174-181.
51. Chappell, B. W., Bryant, C. J. & Wyborn, D. (2012). Peraluminous I-type granites. Lithos, 153, 142-153.
52. Gaudemer, Y., Jaupart, C. & Tapponnier, P. (1988). Thermal control on post-orogenic extension in collision belts. Earth and Planetary Sciences Letters, 89, 48-62.
53. Zhao, Z. F., Gao, P. & Zheng, Y. F. (2015). The source of Mesozoic granitoids in South China: integrated geochemical constraints from the Taoshan batholith in the Nanling Range. Chemical Geology, 395, 11-26.
54. Cai, K. D., Sun, M., Yuan, C., Zhao, G. C., Xiao, W. J., Long, X. P. & Wu, F.Y. (2011). Geochronology, petrogenesis and tectonic significance of peraluminous granites from the Chinese Altai, NW China. Lithos, 127, 261-281.
55. Zhu, R. Z., Lai, S. C., Qin, J. F., Zhao, S. W. & Santosh, M. (2018). Strongly peraluminous fractionated S-type granites in the Baoshan Block, SW China: implications for two stage melting of fertile continental materials following the closure of Bangong Nujiang Tethys. Lithos, 316-317, 178-198
56. Patiño Douce, A. E. (1996). Effects of pressure and H_2O content on the compositions of primary crustal melts. Transactions of the Royal Society, Edinburgh, Earth Sciences, 87, 11-21.
57. Rossi, J. N., Toselli, A. J., Saavedra, J., Sial, A. N., Pellitero, E. & Ferreira, V. P. (2002). Common crustal sources for contrasting peraluminous facies in the early Paleozoic Capillitas Batholith, NW Argentina. Gondwana Research, 5, 325-337.
58. Chen, Y. X., Song, S. G., Niu, Y.L. & Wei, C. J. (2014). Melting of continental crust during subduction initiation: a case study from the Chaidanuo peraluminous granite in the north Qilian suture zone. Geochimica et Cosmochimica Acta, 132, 311-336.
59. Allègre, C. J. & Minster, J. F. (1978). Quantitative models of trace element behavior in magmatic processes. Earth and Planetary Science Letters, 38, 1-25.
60. McKenzie, D. &O'Nions, R. K. (1991). Partial melt distribution from inversion of rare earth element concentrations. Journal of Petrology, 32, 1021–1091.
61. Dawaï, D., Fouotsa, S. A. N., Aboubakar B., Tchameni, R., Nédélec, A. & Bouchez, J. L. (2022). Petrology of the late Pan-African Guider syenite pluton (Cameroon): Implications for magma genesis and emplacement. Journal Africa of Earth Sciences 190:104519

62. Diontar, M., Kwékam, M., Fozing, E. M., Kagou D. A. &Tcheumenak K. J. (2020) Petrology and Geochemical Characteristic of Granitoids From Guéra Massif in the Central Part of Chad: An Example of Mixing Magmas. Earth Science Research, 9-2. https://doi.org/10.5539/esr.v9n2p66.
63. Kwékam, M., Affaton, P., Bruguier, O., Liégeois, J-P., Hartmann, G. & Njonfang, E. (2013) The Pan-African Kekem gabbro-norite (West-Cameroon), U-Pb zircon age, geochemistry and Sr-Nd isotopes: geoadynamical implication for the evolution of the Central Africa fold belt. Journal of African Earth Sciences, 84, 70-88. http://dx.doi.org/10.1016/j.jafrearsci.2013.03.010.
64. Liégeois, J.-P., Navez, J., Hertogen, J. & Black, R. (1998). Contrasting origin of post-collisional high-K calc-alkaline and shoshonitic alkaline and peralkaline granitoids. The use of sliding normalization. Lithos, 45, 1-28. http://dx.doi.org/10.1016/S0024-4937(98)00023-1
65. Pearce, J. A., Harris, N. B. & Tindle, A. G. (1984). Trace element discrimination diagrams for the tectonic interpretation of granitic rocks. Journal of Petrology, 25, 956-983. http://dx.doi.org/10.1093/petrology/25.4.956
66. Forts, B. R. & Lindsley, D. H. (1992). Equilibria among Fe-Ti oxides, pyroxenes, olive and quartz: Part II. Application. American Mineralogist, 77, 1004-1020.
67. Barbarin, B. (1999). A review of the relationships between granitoid types, their origins and their geodynamic environments. Lithos, 46, 605-626. http://dx.doi.org/10.1016/S0024-4937(98)00085-1
68. Wilson, M. (1989). Igneous Petrogenesis. Unwin-Hyman, London, 456p.
69. Sylvester, P. J. (1998). Post-collisional strongly peraluminous granites. Lithos, 45, 29-44.